Hydraulic droplet coarsening in open-channel capillaries

Patrick B. Warren*

Unilever R&D Port Sunlight, Quarry Road East, Bebington, Wirral CH63 3JW, United Kingdom

(Received 21 January 2015; revised manuscript received 17 May 2016; published 14 November 2016)

Over a range of liquid-solid contact angles, an open-channel capillary with curved or angled sides can show a maximum in the Laplace pressure as a function of the filling state. Examples include double-angle wedges, grooves scored into flat surfaces, steps on surfaces, and the groove between touching parallel cylinders. The liquid in such a channel exhibits a beading instability if the channel is filled beyond the Laplace pressure maximum. The subsequent droplet coarsening takes place by hydraulic transport through the connecting liquid columns that remain in the groove. A mean-field scaling argument predicts the characteristic droplet radius $R \sim t^{1/7}$, as a function of time t. This is confirmed by one-dimensional simulations of the coarsening kinetics. Some remarks are also made on the spreading kinetics of an isolated drop deposited in such a channel.

DOI: 10.1103/PhysRevE.94.053111

I. INTRODUCTION

Open channel flow problems have attracted much interest not only because of possible applications in microfluidics [1–9], but also because of the relevance to liquids spreading on topographically patterned surfaces such as human skin [10–12]. The paradigmatic case of spreading in a V-shaped wedge has been analyzed both when liquid is supplied by a reservoir [10,13], and in the starved (no reservoir) situation [14]. Various aspects of these predictions have been confirmed experimentally [2–4,8], and other shapes (e.g., U-shaped microchannels) have been explored for pragmatic reasons [7,11].

Separately, in the study of phase-ordering kinetics [15], Ostwald ripening in systems where the minority phase has a droplet morphology has been of long standing interest since the seminal work by Lifshitz and Slyozov [16], and Wagner [17] (LSW). Of note in this LSW theory is that the droplet radius $R \sim t^{1/3}$, as a function of time t. The one-third exponent (with a possible logarithmic correction in two dimensions [18]) arises because the droplets exchange material by diffusion through the continuous phase. Additionally, in the scaling regime, the droplet size distribution shows scale invariance and is characteristically skewed ('fat-tailed') towards smaller droplets, being truncated above a certain drop size [18,19].

Here, I revisit the problem of droplet coarsening in the context of liquid contained in an open-channel capillary with curved or angled sides. Examples include a V-shaped groove scored into a flat surface Fig. 1(a), a step on a flat surface Fig. 1(b), and the groove formed between a pair of touching parallel cylinders Fig. 1(c). The first two are special cases of two-sided or one-sided double-angle wedges (Fig. 7). The key feature of all these channels is that there is an easily accessible range of contact angles where the Laplace pressure shows a *maximum* as a function of the filling state. Other geometrically simpler channel profiles can exhibit the same phenomenon if there is a gradient in the surface wetting properties. For example, a V-shaped wedge in which the wettability decreases with distance from the apex (so that the contact angle increases) could also display a Laplace pressure maximum.

As shall become clear, above the Laplace pressure maximum a uniform liquid column is unstable towards breaking up into a string of droplets (or 'beads'), similar to Rayleigh's observation of the breakup of a thread of treacle (sugar solution) on a paper surface [20]. Although this instability is by now quite well understood [5,6,9,21–23], I shall argue here that the presence of the Laplace pressure maximum uniquely differentiates this case from previously considered scenarios [24,25], since droplets can coarsen by mass transport through connecting liquid columns. Crucially, this changes the growth law for the characteristic droplet size to $R \sim t^{1/7}$, although many features of the LSW theory are qualitatively preserved.

Below, I shall first present a (long wavelength) stability analysis of the equation governing mass transport in an open-channel capillary to demonstrate the significance of the Laplace pressure maximum in these systems. Subsequently, I shall discuss the consequences for droplet coarsening in the late stages of the beading instability, presenting the mean-field scaling argument which yields the above power law. This result is confirmed by simulations of the one-dimensional coarsening process. Appendix A supports the main text by reporting Laplace pressure *versus* filling state calculations for a selection of channel cross sections. Appendix B supplies the technical details of the simulations. Appendix C considers the related problem of the staged emptying of an isolated droplet into a channel.

The present work focusses on the situation where there is one channel, with a single Laplace pressure maximum as a function of the filling state. More complex situations can certainly be envisaged and will be discussed briefly at the end.

II. WICKING KINETICS

To start with, consider the general problem of open channel flow in a channel of arbitrary cross section, and let $A(x,t)$ be the cross section occupied by liquid where x is the longitudinal direction along the channel. A local mass conservation law holds [13,14,26],

$$\frac{\partial A}{\partial t} + \frac{\partial (A\overline{v})}{\partial x} = 0\,. \tag{1}$$

*patrick.warren@unilever.com

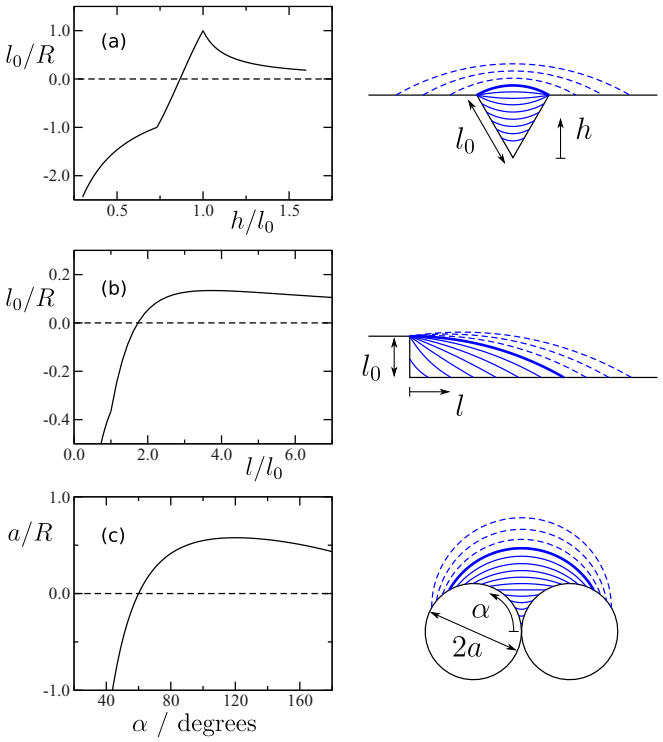

FIG. 1. Examples of open-channel capillaries with a Laplace pressure maximum: (a) V-shaped groove cut into a flat surface (special case of a two-sided double-angle wedge); (b) step on a flat surface (special case of one-sided double-angle wedge); (c) groove between touching parallel cylinders. The left hand plots show the Laplace pressure in reduced units as a function of the filling depth (or a proxy thereof). The right hand diagrams show typical surface profiles (blue). These are circular arcs which meet at a specified contact angle with the surface profile (black lines). The state corresponding to the maximum Laplace pressure is shown as a heavy blue line, and filling states beyond this are shown by dashed lines. Calculations are for a contact angle $\theta = 30^\circ$, and an inner wedge opening angle of $2\phi_1 = 60^\circ$ for case (a). Plots are based on the analytic expressions for the arc radius given in Appendix A. In all cases the area A is monotonically increasing with the chosen measure of filling depth.

Herein the mean flow rate $\overline{v}$ satisfies a Hagen-Poiseuille (HP) law, $\overline{v} = -(k/\eta)\,\partial p/\partial x$, in which $k(A)$ is an area-dependent hydraulic conductivity, η is viscosity, and $p = p(A)$ is the area-dependent Laplace pressure (the hydraulic conductivity is a quantity with units of length squared, cf. Darcy's law). Combining the HP law with Eq. (1) gives a self-contained equation for $A(x,t)$,

$$\frac{\partial A}{\partial t} = \frac{\partial}{\partial x}\left(\frac{Ak}{\eta}\frac{dp}{dA}\frac{\partial A}{\partial x}\right). \tag{2}$$

Equation (2) generally has the character of a non-linear diffusion equation. I have assumed that the occupied cross section A is weakly varying with x, so the contribution to the Laplace pressure from the interface curvature in the longitudinal direction can be neglected. Technically this means the equation is valid only for long wavelength perturbations (but see also below).

Insight can be gained by linearising about the uniform static solution, viz. $A = A_0$ and $\overline{v} = 0$. Let us write $A/A_0 = 1 + \epsilon(x,t)$. Then $\partial\epsilon/\partial t = D_{\text{eff}}\,\partial^2\epsilon/\partial x^2$ where $D_{\text{eff}} = (Ak/\eta)\,dp/dA$ is an effective diffusion coefficient, evaluated at $A = A_0$. It is clear that the sign of D_{eff} is governed by the sign of dp/dA (and not p), and this therefore differentiates between two different behaviors. If $dp/dA > 0$ ($D_{\text{eff}} > 0$) an initial height perturbation will die out. In this situation an overfilled region ($A > A_0$) has a higher Laplace pressure than an underfilled region, and liquid will flow to iron out an initial perturbation. On the other hand if $dp/dA < 0$ ($D_{\text{eff}} < 0$) an initial height perturbation will grow exponentially. In this situation liquid flows from underfilled regions into overfilled regions, amplifying the initial imbalance. The unusual property of a channel with a Laplace pressure maximum is that *both* behaviors can occur (Fig. 2), depending on the filling state. This has important and interesting consequences for the kinetics and is the central message of the present work.

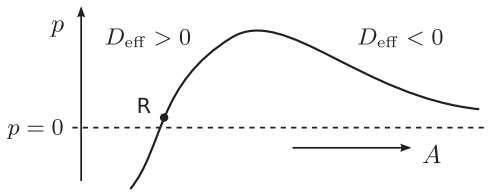

FIG. 2. Schematic Laplace pressure curve, $p(A)$, with a maximum. The abscissa at $p = 0$ is indicated by the dashed line.

For pragmatic reasons it is often convenient to use a filling depth h (or a suitable proxy thereof) instead of the area A, as in Fig. 1. Provided $A(h)$ is a monotonic increasing function ($dA/dh > 0$) the above arguments can also be couched in terms of dp/dh.

III. BEADING INSTABILITY

Suppose one starts with a channel initially uniformly filled in a filling state beyond the Laplace pressure maximum. Since $dp/dA < 0$, this uniform state is unstable by the above argument, and small perturbations will start to grow, initially exponentially. As in the Rayleigh problem [27], I expect that the fastest growing instability mode will have a length scale set by a characteristic filling depth h_0 [20,27,28]. After this initial exponential growth phase the kinetics becomes non-trivial, but by analogy to the behavior of liquid jets [25], I expect the liquid contained in the channel will ultimately take the form of a string of droplets, in this case connected by stable thin liquid columns. Assuming the fastest growing instability mode selects the structure, one might expect the mean droplet size and spacing to be set also by h_0.

The actual droplet size and spacing at this point will be slightly non-uniform, reflecting slight inhomogeneities in the initial state. Thus this droplet state itself is susceptible to further coarsening by hydraulic transport through the connecting liquid columns. Large droplets will grow at the expense of the smaller ones, which will shrink and disappear. Eventually in the final state a single large droplet will exist somewhere on the channel. This is a necessary condition for stability since two or more coexisting droplets on the right hand

side of the Laplace pressure maximum in Fig. 2 are unstable with respect to an exchange of liquid volume.

In this final state, the large droplet containing the excess liquid will assume some three-dimensional profile concomitant with the boundary conditions. The Laplace pressure in the droplet will be slightly positive in comparison to typical channel Laplace pressure, since the droplet is large compared to the channel dimensions. Since this is supposed to be the final static condition, the liquid column in the channel must be at the *same* slightly positive Laplace pressure as the droplet, and will therefore correspond to a filling state just above the zero-crossing of the $p(A)$ curve (e.g., point R in Fig. 2) [29].

This hydraulic coarsening mechanism stands in contrast to the behavior of droplets in a V-shaped wedge for example, where spatially separated droplets are disconnected [4,30,31] and the droplet population has to coarsen by some other mechanism, such as a prewetting film [32–34], or transport through the vapor phase in the case of a volatile liquid (see below).

I now consider the late-stage coarsening kinetics: how is this final single-large-droplet state arrived at, starting from a string of droplets in the channel? After the initial stages of the beading instability, I envisage an evolving droplet size distribution with a diminishing number of droplets, very much like the situation for Ostwald ripening mentioned in the introduction. The characteristic filling depth h_0 of the connecting liquid columns will be such that $p(A) \approx 0$ (in the examples in Fig. 1 one has $h_0 \sim l_0$ for the double-angle wedges, or $h_0 \sim a$ for touching parallel cylinders). This is because locally the liquid columns are connected to droplets with a weakly positive Laplace pressure (cf. Fig. 2), noting that at late stages $R \gg h_0$. As already mentioned, unless the channel is grossly overfilled, h_0 is also the relevant length scale for the fastest growing mode in the initial instability so that the initial droplets will have a volume of order h_0^3, and spacing of order h_0.

With this picture, I now argue that aspects of the LSW theory can be adapted to the late stage coarsening kinetics in the present problem, where there is an evolving population of droplets. I make the simplifying assumption that the Laplace pressure scales inversely with droplet volume, viz. $p \propto V^{-1/3}$, where $V \sim R^3$. This is likely to be true only asymptotically [35,36]. Nonetheless, let us suppose that this is true, then following mean-field scaling argument predicts how the characteristic droplet size R, and characteristic spacing between droplets L, evolve with time.

First, the mass flux between adjacent droplets is order

$$J \sim \frac{h_0^4}{\eta}\frac{\Delta p}{L}. \tag{3}$$

This just expresses the HP law in scaling form. The fourth power of h_0 arises from the product of the hydraulic conductivity $k \sim h_0^2$ and the cross sectional area of the connecting liquid column $A \sim h_0^2$.

The mass flux is incorporated into a *local* mass conservation law, cf. Eq. (1), according to which

$$\frac{dV}{dt} \sim J. \tag{4}$$

At the same time there is a *global* mass conservation law which relates the characteristic droplet volume to the characteristic droplet spacing,

$$\frac{V}{L} \sim \omega\,, \tag{5}$$

where ω is the mass (volume) per unit length, which is *constant* and fixed by the initial conditions. Typically one might expect $\omega \sim h_0^2$, unless the channel is grossly overfilled.

Combining Eqs. (3)–(5), together with $V \sim R^3$ and $\Delta p \sim \gamma/R$ (where γ is the surface tension), shows that

$$R^2\frac{dR}{dt} \sim \frac{\gamma h_0^4 \omega}{\eta R^4}\,. \tag{6}$$

This integrates to

$$R \sim h_0\left(\frac{\gamma\omega t}{\eta h_0^3}\right)^{1/7} \text{ or } R \sim h_0\left(\frac{\gamma t}{\eta h_0}\right)^{1/7} \tag{7}$$

(the second case assumes $\omega \sim h_0^2$). This yields the claimed $R \sim t^{1/7}$ growth law. The additional prediction is that the droplet line density (i.e., $L^{-1} \sim R^{-3}$) should diminish as $t^{-3/7}$. To make sense of this note that γ/η is a velocity [36], and for example a 10 cSt oil ($\eta \approx 10\,\text{mPa s}$, $\gamma \approx 10\,\text{mN m}^{-1}$) has γ/η of order $1\,\text{ms}^{-1}$. If $h_0 \approx 100\,\mu\text{m}$ the relevant time scale $\eta h_0/\gamma$ is of the order $100\,\mu\text{s}$. Thus on a time scale of seconds one expects to be well into the hydraulic droplet coarsening regime, with a characteristic droplet size several times the channel dimensions.

One might be concerned that other coarsening mechanisms might intervene to destroy this result. Indeed, there are two processes which might lead to droplet coalescence. The first is that growing droplets could bump into their neighbours and swallow them up. However such direct contacts become vanishingly rare since the ratio between the characteristic droplet size and characteristic droplet spacing, $R/L \sim t^{-2/7}$. This is $O(1)$ initially and diminishes with time. Thus I would not expect droplet coalescence by this process to be significant.

The second process that could lead to droplet coalescence is droplet migration. In general there is an imbalance in the flux in the two liquid columns connected to a droplet. To avoid becoming 'misshapen' (i.e., having a non-constant interface curvature), the droplet will have to redistribute liquid from one side to the other. This shape relaxation will be fast on the time scale of the coarsening process since the hydraulic conductivity of the droplets ($k \sim R^2$) is significantly larger than the connecting liquid columns ($k \sim h_0^2$). In general it will lead to a displacement of the center of mass of the droplet, by a distance $O(R)$, at most. This corresponds to an effective droplet migration mechanism. But as we have noted R/L is $O(1)$ initially and diminishing, so the migration distances involved are small compared to the droplet spacing, and this process should also be irrelevant for the late stage coarsening kinetics.

For volatile liquids, transport through the vapor phase is a third possibility. This is potentially relevant, and would lead to the return of the LSW scaling law $R \sim t^{1/3}$. Moreover, as long as the vapor-phase diffusion is three-dimensional, it should not matter whether the droplets are arrayed in a one-dimensional string or placed at random on a two-dimensional surface. This is because the mean-field *ansatz* underpinning the LSW theory 'washes out' such spatial information. The

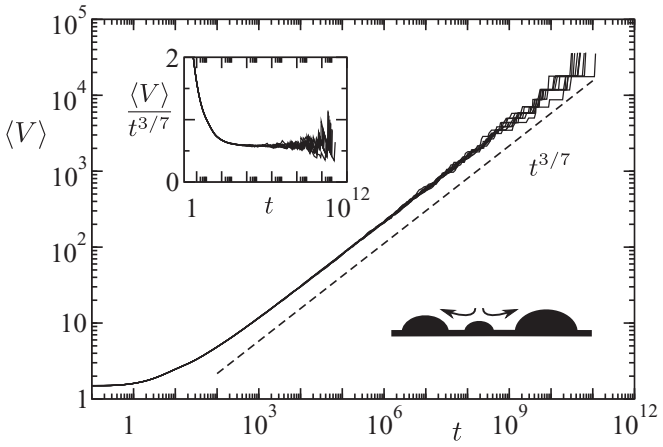

FIG. 3. Mean droplet volume as a function of time, from simulation. Droplets coarsen by hydraulic transport along the connecting liquid columns (lower schematic inset), according to the rules prescribed in Appendix B. Results from ten independent simulation runs are shown. Each simulation was initialized with $N_0 = 5\times10^4$ equispaced droplets, with random sizes taken from a uniform distribution $V_0 < V < 2V_0$. Droplets are removed when $V < 0.9\,V_0$, and their liberated contents are added to the liquid column ($\beta = 1$ in the model). The adaptive integration control parameter was $\epsilon = 0.02$.

diffusive $t^{1/3}$ law grows faster than the hydraulic $t^{1/7}$ law. So, eventually, diffusive transport should dominate and diffusion-controlled Ostwald ripening should take over. Of course the point where this happens depends on the material properties and in particular on the volatility of the liquid. For a nominally non-volatile liquid one would expect a large regime where hydraulic droplet coarsening should be observable.

Since mean field arguments are notoriously unreliable in one-dimensional systems, it seems prudent to verify the above mean-field theory prediction. To investigate specifically this aspect therefore, I undertook numerical simulations of a string of $i = 1 \ldots N$ droplets of volumes V_i, using the model described in Appendix B. As time advances, the larger droplets grow at the expense of the smaller droplets, and the smallest droplets shrink and vanish. Eventually the simulation stops when there is one large final droplet ($N = 1$). I monitor the mean droplet volume $\langle V \rangle = (1/N)\sum_{i=1}^{N} V_i$ as a function of time (note that N changes as droplets disappear), and at selected time points record the drop size distribution. I also calculate at various elapsed simulation times the equal-time correlation function, $C(|i-j|,t) = \langle \Delta V_i\, \Delta V_j \rangle / \langle \Delta V^2 \rangle$, where $\Delta V_i = V_i - \langle V \rangle$ is the deviation from the mean droplet volume, at time t. Note that $|i-j|$ is the distance between droplets, measured in terms of the number of connecting liquid columns.

Typical results, aggregated from multiple simulation runs from independent starting points, are summarized in Figs. 3 and 4 (Fig. 8 shows that the results are robust to changes in the simulation parameters). Figure 3 demonstrates that the mean-field scaling argument does indeed predict how the mean droplet size grows with time. Alongside this, Fig. 4 demonstrates scale invariance holds for the droplet size distribution. The latter shares some characteristic features with LSW theory [15,18]: there is an obvious skew asymmetry

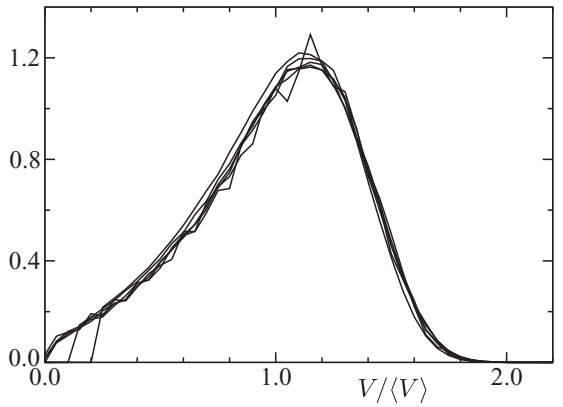

FIG. 4. Scale invariance of droplet size distribution, when there are 10 000, 5000, 1000, 500, 300, and 100 droplets remaining (out of an initial 5×10^4 droplets). Data are combined from 100 independent simulation runs. Simulation parameters as for Fig. 3.

towards smaller droplet sizes, the distribution is apparently truncated beyond a certain droplet size (in this case for $V \gtrsim 2\,\langle V \rangle$), and there is a 'fat tail' of smaller droplets.

The origin of the mean-field behavior is apparent if one examines the equal-time droplet size correlation function, $C(|i-j|,t)$, shown in Fig. 5. As can be seen the only significant correlation that develops is between nearest neighbors, at $|i-j| = 1$. This indicates that droplets which are larger than average tend to be adjacent to droplets which are smaller than average, but apart from this no significant long-range correlations develop.

To see the origin of this short-range correlation, consider an artificial situation in which one large droplet sits in a uniform one-dimensional array of equisized smaller droplets. Away from the large droplet, the ambient Laplace pressure is uniform and no coarsening takes place. However the large droplet has a sub-ambient Laplace pressure and so starts to draw liquid from its immediate neighbors. This causes the immediate neighbors to shrink, and increases their Laplace pressure relative to the ambient background. The next-nearest neighbors then see this, and so they in turn start to grow at the expense of the shrinking

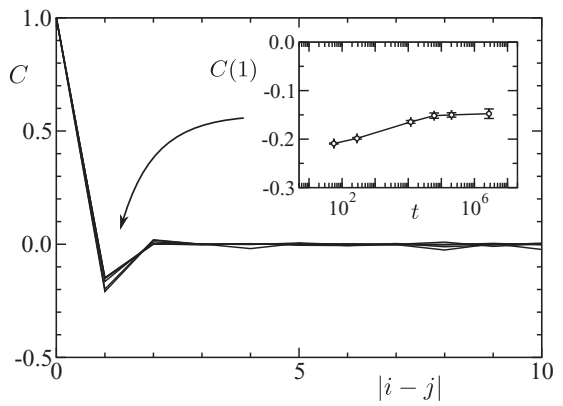

FIG. 5. Equal-time size correlation function, $C(|i-j|,t)$, computed for the same set of simulations used for Fig. 4. The inset shows the time dependence of the depth of the nearest-neighbour minimum. Error bars are from block averaging (10 blocks × 10 runs).

nearest neighbors. It is easy to see that this will drive a negative nearest-neighbor size correlation.

The nearest-neighbor correlation minimum diminishes somewhat as time progresses, but eventually appears to settle down to a value $C(1) \approx -0.15$ (Fig. 5 inset). I should point out that the coarsening dynamics in the model is quite subtle, for instance, the largest droplet at time t may not necessarily be the largest droplet at some later time $t' > t$. This is because the growth rate of a droplet depends not only on its size but also on the sizes of its neighbors, and how far away they are.

IV. DISCUSSION

The present work examines droplet coarsening in open-channel capillaries which exhibit a maximum in the Laplace pressure as a function of filling state (typically, channels with curved or angled sides). I argue that the kinetics is fundamentally modified because droplets can exchange material by hydraulic transport along connecting liquid columns. The difference is sufficient to change qualitatively the growth law compared to diffusion-controlled Ostwald ripening. With a simplifying assumption about the dependence of the Laplace pressure on the droplet volume, a mean-field scaling argument can be used to obtain the growth law. The mean-field theory is validated by simulations.

Of course, in general I would expect the clean power-law behavior to be modified by finite-size effects arising from the precise dependence of the Laplace pressure on the droplet volume. These may be quite persistent. Some general predictions should be robust however, such as the relatively rapid deceleration in the droplet growth rate, and the negative correlation between nearest neighbor droplet sizes shown in Fig. 5. These could perhaps be tested in experimentally.

For the present droplet coarsening problem there are a couple of obvious avenues for future work. First, a more detailed analysis of the coarsening kinetics could be undertaken using the methods developed for diffusion-controlled Ostwald ripening [15,18,19]. The main aim of this would be to recover the droplet size distribution scaling function seen in Fig. 4. Second, precise calculations of interface morphologies in specific channel geometries could be undertaken to examine the particular dependence of the Laplace pressure on droplet size. Possible methodologies to do this include surface evolver [37], coarse-grained molecular dynamics [38], phase-field simulations [39], and lattice Boltzmann [40].

More generally, outside the range of contact angles where the Laplace pressure exhibits a single maximum, a complex 'zoo' of stable liquid droplet morphologies can ensue. This is discussed for example in the case of a surface step by Brinkmann and Blossey [41]. It is perhaps worth noting that no stable static droplet states exist in the channel *within* the range of contact angles considered in the present work. Indeed, an isolated droplet deposited into the channel would simply empty into the unfilled regions. This is an interesting problem in its own right, and is examined in more detail in Appendix C. Again, this may perhaps be probed experimentally.

Additionally, one can also envisage a situation where the Laplace pressure $p(A)$ exhibits multiple extrema. A practical example relevant to the present geometries would arise if the apex is *blunted*, perhaps as a manufacturing artefact. In such a geometry, the Laplace pressure may show a local minimum before diverging ($p \to \infty$) as $A \to 0$ (Fig. 6). In actual fact, this does not obviously destroy the droplet coarsening physics envisaged in the present work as long as the droplets and connecting liquid columns remain on the weakly positive Laplace pressure branch of the curve (i.e., to the right of point R in Fig. 6). In particular, note that the connecting liquid columns live on the branch of the curve where $dp/dA > 0$ ($D_{\text{eff}} > 0$), and should therefore be mechanically stable. Under a large perturbation though, a connecting liquid column may be severed, at which point I would expect the severed ends to withdraw into the nearest macroscopic droplets. These macroscopic terminal droplets would then exhibit a complex morphology driven by need to accommodate a constant interface curvature, at fixed contact angle, in the complex geometry of the groove.

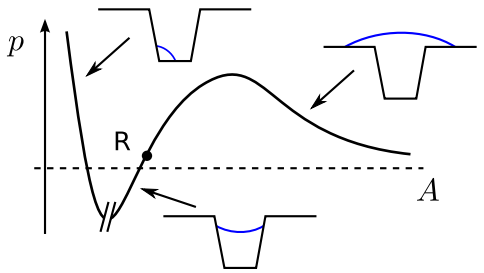

FIG. 6. Laplace pressure curve with multiple extrema, which could arise for a *blunted* V-shaped surface groove (insets). The divergence at $A \to 0$ corresponds to a filling state with broken symmetry that lives in one of the corners of the channel. Note that such a state would be mechanically unstable ($dp/dA < 0$) [30]. The hiatus in the curve is meant to signify that multiple branches of $p(A)$ may be possible in the transition region, where a given cross-sectional area may correspond to more than one filling state.

While droplet coarsening in these channels is naturally one-dimensional ($d = 1$), one can also envisage a two-dimensional ($d = 2$) analog where droplets coarsen on a planar surface crisscrossed by such channels, such as steps or V-shaped grooves. Naïvely the global mass conservation law in Eq. (5) generalizes to $V/L^d \sim \omega$, and this is the only change that needs to be made. This leads to a more general $R \sim t^{d/(3+4d)}$ growth law (thus $R \sim t^{2/11}$ for $d = 2$). However, at least one additional length scale bears on the two dimensional coarsening problem, namely the mean groove spacing (or the groove length per unit area). This complicates the analysis of the two-dimensional case, which is left for future work.

APPENDIX A: STATICS

To support the discussion in the main text, I present results for the Laplace pressure curves for selected channel cross sections. In the long-wavelength limit of Eq. (2), the interface curvature is negligible in the longitudinal direction and the transverse profile is an arc of a circle with radius R. Taking $R > 0$ to indicate the surface is convex outwards, the Laplace pressure is $p = \gamma/R$ where γ is surface tension. The calculation of $p(A)$ is therefore reduced to the calculation of R, which is essentially a problem in Euclidean plane geometry. Some example plots of $1/R$ as a function of filling depth h

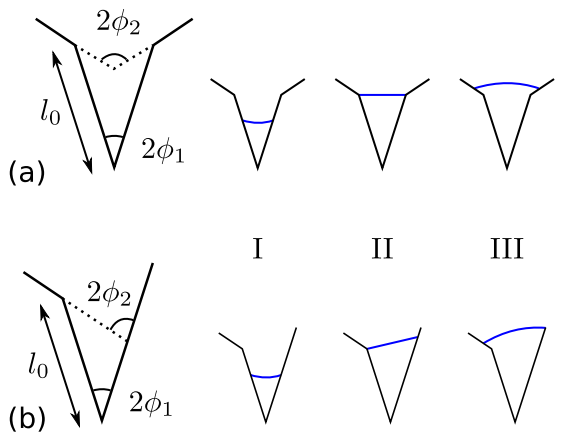

FIG. 7. (a) Two-sided and (b) one-sided double-angle wedges, with the three filling regimes illustrated.

(or a proxy thereof) are shown in Fig. 1. Note that in all cases $A(h)$ is obviously monotonic ($dA/dh > 0$).

Two-sided double-angle wedge—The general shape I have in mind is shown in Fig. 7(a), where the inner and outer wedge half-angles are ϕ_1 and ϕ_2, respectively. For a liquid in a V-shaped wedge it has long been known that the Laplace pressure is positive (negative) as $\theta + \phi - \frac{1}{2}\pi$ is positive (negative), where θ is the liquid-solid contact angle [30]. To ensure a maximum in $p(h)$ I shall therefore consider the range of contact angles where $\frac{1}{2}\pi - \phi_2 < \theta < \frac{1}{2}\pi - \phi_1$. Then, there are three regimes as the filling depth increases (Fig. 7(a), right hand diagrams). In regime I the liquid is contained solely in the inner wedge and p is a negative increasing function of h. In the intermediate regime II the contact line is pinned at the convex corners and p monotonically increases with h, crossing through zero when the interface is flat. In regime III the contact line has depinned from the convex corners to enter the outer wedge, and p is now a positive decreasing function of h. Taken together therefore, the maximum in $p(h)$ occurs when the contact line depins at the II-III regime cross over.

To quantify this, I first note that the channel profile is characterized by a single length scale which can be taken to be the length l_0 of the side of the inner wedge Fig. 7(a). Let $\theta' = \theta + \phi_2 - \phi_1$ be the *apparent* contact angle for the *inner* wedge, at the point where the contact line depins to enter the *outer* wedge. Then the I–II and II–III crossovers are, respectively, at filling depths

$$\begin{aligned} h_1 &= l_0 \times [\cos\theta - \sin\phi_1]/\cos(\theta + \phi_1), \\ h_2 &= l_0 \times [\cos\theta' - \sin\phi_1]/\cos(\theta' + \phi_1). \end{aligned} \tag{A1}$$

It is also helpful to introduce the offset between the apex of the inner wedge and the extrapolated apex of the outer wedge, $x_{\text{off}} = l_0 \sin(\phi_2 - \phi_1)/\sin\phi_2$, and the offset filling depth $h' = h - x_{\text{off}}$. In these terms the interface curvature (i.e., the Laplace pressure in reduced units) is given by

$$\frac{1}{R} = \begin{cases} (\sin\phi_1 - \cos\theta)/(h\sin\phi_1) & \text{(I)}, \\ \dfrac{2(h - l_0\cos\phi_1)}{l_0^2 + h^2 - 2l_0 h\cos\phi_1} & \text{(II)}, \\ (\sin\phi_2 - \cos\theta)/(h'\sin\phi_2) & \text{(III)}. \end{cases} \tag{A2}$$

One can check that this is a piecewise continuous function (of h). The zero crossing is obviously at $h = l_0\cos\phi_1$. Note that $\phi_2 = \frac{1}{2}\pi$ corresponds to the interesting special case shown in Fig. 1(a) where a V-shaped groove (the inner wedge) is scored into a flat surface (the outer wedge).

One-sided double-angle wedge—The one-sided double-angle wedge has a convex corner only on one side (Fig. 7 b). I shall again assume that $\frac{1}{2}\pi - \phi_2 < \theta < \frac{1}{2}\pi - \phi_1$ so, at the risk of belaboring the point, the same three filling regimes obtain as for the previous case. Because of the asymmetry it is more convenient in this case to use the wetted length l of the unbroken side as a proxy for the filling depth. The corresponding I–II and II–III regime crossovers are at, respectively,

$$\begin{aligned} l_1 &= l_0, \\ l_2 &= x_{\text{off}} + l_0 \times \sin(2\phi_1)/\sin(2\phi_2), \end{aligned} \tag{A3}$$

where the apex offset here is $x_{\text{off}} = l_0\sin(2\phi_2 - 2\phi_1)/\sin(2\phi_2)$. Defining $l' = l - x_{\text{off}}$, the interface curvature in this case is

$$\frac{1}{R} = \begin{cases} -\cos(\theta + \phi_1)/(l\sin\phi_1) & \text{(I)}, \\ \dfrac{2[l\sin\theta - l_0\sin(\theta + 2\phi_1)]}{l_0^2 + l^2 - 2l_0 l\cos(2\phi_1)} & \text{(II)}, \\ -\cos(\theta + \phi_2)/(l'\sin\phi_2) & \text{(III)}. \end{cases} \tag{A4}$$

Again this is a piecewise continuous function (of l). The zero crossing is at $l = l_0 \times \sin(\theta + 2\phi_1)/\sin\theta$. The maximum can occur either when the interface depins from the convex corner (the II–III crossover), or (perhaps unexpectedly) within regime II at an intermediate filling depth $l = l_0 \times \sin(\frac{1}{2}\theta + 2\phi_1)/\sin\frac{1}{2}\theta$. Geometrically this corresponds to the point where the inner wedge apparent contact angle $\theta' = \pi - 2\phi_1$, so that the tangent to the surface at the pinned contact line is parallel to the opposite side of the wedge.

The case $\phi_2 = \frac{1}{2}\pi$ generates the step geometry considered by Brinkmann and Blossey [41] (their $\alpha = 2\phi_1$). When further $\phi_1 = \frac{1}{4}\pi$ one has as a special case a vertical step on a flat surface Fig. 1(b). Brinkmann and Blossey note that $\theta < \frac{1}{2}\pi - \phi_1$ corresponds to complete spreading of the liquid along the bottom edge of the step, in agreement with the present analysis. Note that in the case $\phi_2 = \frac{1}{2}\pi$ the contact line can never depin from the convex corner, since a circle cannot intersect displaced parallel lines at the same angle [42]. Regime III therefore is not encountered, and the Laplace pressure maximum (if it occurs) is in regime II.

Touching parallel cylinders—In this problem it is convenient to parametrize the filling depth by the wrapping angle α [9]. Again, the geometry is characterized by a single length scale which I shall take to be the cylinder radius a. Elementary trigonometric arguments, first presented to my knowledge by Princen [21], show that

$$\frac{a}{R} = -\frac{\cos(\theta + \alpha)}{1 - \cos\alpha}. \tag{A5}$$

The sign has been inserted in accord with the above convention that R is positive if the interface is convex. From this one finds

(after a little rearrangement)

$$\frac{dR}{d\alpha} = -\frac{R^2 \cos\left(\frac{1}{2}\alpha + \theta\right)}{2a \sin^3\left(\frac{1}{2}\alpha\right)} . \tag{A6}$$

Taken together, Eqs. (A5) and (A6) show that zero crossing of $p(\alpha)$ is at $\alpha = \frac{1}{2}\pi - \theta$, and there is a weak maximum at $\alpha = \pi - 2\theta$.

An interesting observation in this problem is that the maximum stable filled state will protrude above the cylinders if $\theta < \frac{1}{3}\pi$ (=60°), and the more the contact angle is reduced, the higher the stable filled state protrudes. The behavior stands in marked contrast to the influence of contact angle on the height of a droplet sitting as a spherical cap on a flat surface. This consideration potentially influences the wicking of liquids in woven fibrous materials.

APPENDIX B: SIMULATION DETAILS

Figures 3–5 in the main text validate the mean-field scaling predictions. Here I describe the technical details of the underpinning simulations. The model describes the time evolution of a one-dimensional string of $i = 1 \ldots N$ droplets, connected by liquid columns as indicated in the lower schematic inset in Fig. 3. Big droplets grow, and small droplets shrink, under the influence of hydraulic transport through the liquid columns driven by differences in the Laplace pressure between neighboring droplets. To establish a system of kinetic equations for the droplet sizes, I suppose that the Laplace pressure in the ith droplet is proportional to $V_i^{-1/3}$, where V_i is the droplet volume (this is the simplifying assumption mentioned in the main text). According to the HP law, the Laplace pressure difference drives a mass flux through the connecting liquid column as, cf. Eq. (3),

$$J_i = \frac{V_i^{-1/3} - V_{i+1}^{-1/3}}{L_i} . \tag{B1}$$

In this L_i is the distance between the ith and $(i+1)$th droplets, and all other material properties in the problem have been subsumed into the definitions of length, volume, and time. Note that $V_{i+1} > V_i$ implies $J_i > 0$, so that liquid flows from smaller droplets to larger droplets. Given the fluxes, mass conservation dictates that, cf. Eq. (4),

$$\frac{dV_i}{dt} = J_{i-1} - J_i . \tag{B2}$$

Equations (B1) and (B2) are the required set of non-linear kinetic equations. Since they predict that droplets shrink, as well as grow, we need a rule which governs how shrinking droplets can disappear. At this point it is convenient to introduce a fiducial volume $V_0 \sim h_0^3$, where h_0 is the characteristic filling depth described in the main text (in the simulations, $V_0 = h_0 = 1$). A simple rule for shrinking droplets is that they vanish when $V_i < \alpha V_0$. If this happens, the droplet is removed and the distance between the remaining droplets is set equal to $L_{i-1} + L_i + \beta V_i^{1/3}$, where the third term is an *ad hoc* correction for the length contributed by the vanished droplet (taking β as a free parameter).

The droplet volumes are evolved according to Eqs. (B1) and (B2), alongside the rule for removing droplets which become too small. The kinetic equations are integrated using a simple, adaptive, Euler-type forward finite difference scheme, with a time step Δt chosen such $dV_i/dt \times \Delta t / V_i \leqslant \epsilon$, in other words so that the fractional change in any droplet size does not exceed ϵ in any time step. As an initial condition I set $V_i = r_i V_0$ where r_i is a random number chosen from a uniform distribution, $1 \leqslant r_i < r_m$. The droplets are initially equispaced, with $L_i = h_0$. Periodic boundary conditions are imposed.

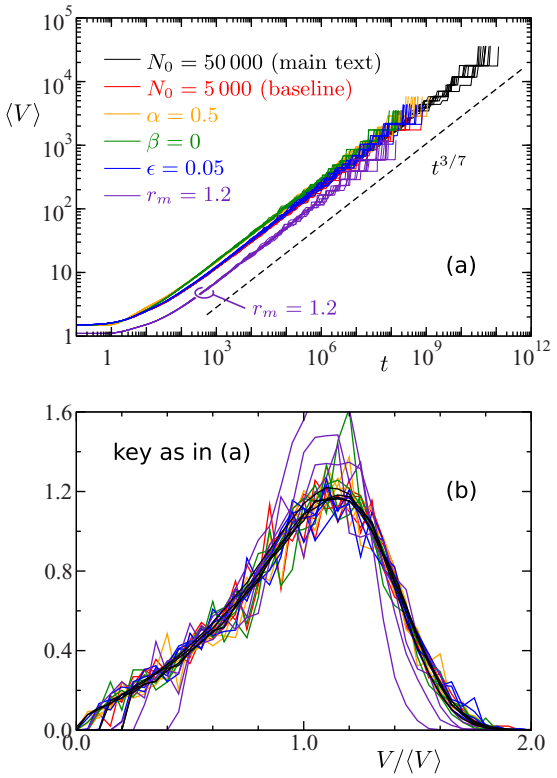

FIG. 8. Effect of changing parameters in the simulation on (a) the evolution of the mean droplet volume with time and (b) the drop size distribution. The baseline is $N_0 = 5000$, $\alpha = 0.9$, $\beta = 1$, $\epsilon = 0.02$, and $r_m = 2$, where N_0 is the initial number of droplets. In (a) the outlier at $r_m = 1.2$ is lassoed. In (b) the size distribution is sampled when there are 1000, 500, 300, and 100 droplets remaining and, apart from the main text result where 100 runs were used, data is combined from ten independent simulation runs for each variant.

The results reported in Figs. 3–5 in the main text used $\alpha = 0.9$ and $\beta = 1$ for the vanishing rule, $r_m = 2$ for the maximum initial drop size relative to V_0, and $\epsilon = 0.02$ for the adaptive integration scheme. Figure 8 demonstrates that the results are insensitive to these choices. Note that if r_m is decreased, the initial droplet size distribution becomes narrower, and it takes longer for the full scaling behavior to be attained.

APPENDIX C: DROPLET SPREADING KINETICS

As noted in the main text, the fate of a droplet of liquid deposited onto an initially empty channel is an interesting problem in its own right. The existence of a Laplace pressure maximum implies that a large enough droplet should show *staged* spreading kinetics as it empties into the unfilled

channel. This may be relevant to applications such as oily soil spreading along the fibres in textile yarns in woven fabrics, and wicking of molten solder in stranded copper wires and braids.

I shall suppose that the droplet is large enough so that the initial filling state is above the Laplace pressure maximum. In this case the negative effective diffusion coefficient ($D_{\text{eff}} < 0$) suppresses the tendency for the droplet to spread out. Therefore I expect that initially the droplet will assume a quasi-static shape, but will also immediately start to empty into the channel driving a Bell-Cameron-Lucas-Washburn (BLCS) type flow from what is in effect a shrinking droplet reservoir [10,13,26]. In this early stage therefore I expect to find an $L \sim t^{1/2}$ spreading law (BLCS). This should persist all the way until the filling falls below the Laplace pressure maximum. Past this point, and by analogy to the V-shaped wedge [14], one expects the spreading rate to slow down since the reservoir has been exhausted.

In this second stage, power-law spreading may be recovered, but with a non-trivial exponent. For the case of a double-angle wedge, by this point the liquid is entirely contained within the inner wedge and $L \sim t^{2/5}$ should be observed [14]. However for the case of a groove between touching parallel cylinders, I would not expect a power law to appear until the very late stages where everywhere the wrapping angle $\alpha \ll 1$. To analyze this specific situation (i.e., late stage spreading in the groove between touching parallel cylinders), a scaling analog of the HP law can be introduced: $dL/dt \sim (k/\eta) \times \Delta p/L$, where $\Delta p \sim \gamma/R$ is the Laplace pressure. In the limit in which we are interested, the wetted portion of the groove has shrunk to a narrow fissure with a width of the order $R \sim \alpha^2 a$ [see Eq. (A5) in the limit $\alpha \to 0$] and a depth of the order αa. One therefore expects $k \sim \alpha^4 a^2$ since the hydraulic conductivity is presumably determined by the width. Substituting these in the HP scaling law gives $dL/dt \sim \gamma \alpha^2 a/(\eta L)$. An additional constraint comes from the analog of the global mass conservation law in Eq. (5), namely that the total droplet volume Ω should be conserved. Again, in this limiting case the cross section area $A \sim \alpha^3 a^2$ and therefore $\Omega \sim \alpha^3 a^2 L$. Eliminating α between the volume constraint $d\Omega/dt = 0$ and the HP scaling law yields $dL/dt \sim \gamma \Omega^{2/3}/(\eta a^{1/3} L^{5/3})$. This integrates to the final rather esoteric result $L \sim (\gamma t/\eta)^{3/8}\, \Omega^{1/4}\, a^{-1/8}$. In other words, for a droplet deposited into the groove between touching parallel cylinders, the initial $L \sim t^{1/2}$ spreading law (BLCS) should weaken when the droplet reservoir vanishes, and eventually cross over to an $L \sim t^{3/8}$ power law in the final starved state.

[1] T. M. Squires and S. R. Quake, Rev. Mod. Phys. **77**, 977 (2005).
[2] J.-C. Baret, M. M. J. Decré, S. Herminghaus, and R. Seemann, Langmuir **23**, 5200 (2007).
[3] K. Khare *et al.*, Langmuir **23**, 12997 (2007).
[4] K. Khare *et al.*, Eur. Phys. J. Special Topics **166**, 151 (2009).
[5] X.-F. Wu, A. Bedarkar, and K. A. Vaynberg, J. Colloid Interface Sci. **341**, 326 (2010).
[6] A. Bedarkar, X.-F. Wu, and A. Vaynberg, Appl. Surf. Sci. **256**, 7260 (2010).
[7] D. Yang *et al.*, J. Phys. Chem. C **115**, 18761 (2011).
[8] J. Barman *et al.*, Langmuir **31**, 1231 (2015).
[9] A. Sauret *et al.*, Soft Matter **11**, 4034 (2015).
[10] A. D. Dussaud, P. M. Adler, and A. Lips, Langmuir **19**, 7341 (2003).
[11] Y. Chena *et al.*, Micro. Engn. **86**, 1317 (2009).
[12] R. Seemann *et al.*, J. Phys.: Condens. Matter **23**, 184108 (2011).
[13] L. A. Romero and F. G. Yost, J. Fluid Mech. **322**, 109 (1996).
[14] P. B. Warren, Phys. Rev. E **69**, 041601 (2004).
[15] A. J. Bray, Adv. Phys. **43**, 357 (1994).
[16] I. M. Lifshitz and V. V. Slyozov, J. Phys. Chem. Solids **19**, 35 (1961).
[17] C. Wagner, Z. Elektrochem. **65**, 581 (1961).
[18] J. H. Yao, K. R. Elder, H. Guo, and M. Grant, Phys. Rev. B **45**, 8173 (1992).
[19] J. H. Yao, K. R. Elder, H. Guo, and M. Grant, Phys. Rev. B **47**, 14110 (1993).
[20] Lord Rayleigh, Phil. Mag. **34**, 145 (1892).
[21] H. M. Princen, J. Colloid Interface Sci. **34**, 171 (1970).
[22] A. E. Sáez and R. G. Carbonell, J. Fluid Mech. **176**, 357 (1987).
[23] C. Duprat, A. D. Bick, P. B. Warren, and H. A. Stone, Langmuir **29**, 7857 (2013).
[24] S. Chandrasekhar, *Hydrodynamic and Hydromagnetic Stability* (Dover, New York, 1981).
[25] J. Eggers, Rev. Mod. Phys. **69**, 865 (1997); J. Eggers and E. Villermaux, Rep. Prog. Phys. **71**, 036601 (2008).
[26] M. Reyssat, L. Courbin, E. Reyssat, and H. A. Stone, J. Fluid Mech. **615**, 335 (2008).
[27] A crucial point is that the friction against the substrate engenders breakup into droplets with a characteristic size and spacing set by the initial diameter of the liquid column. This is in contrast to the viscous breakup of a free-standing liquid column, which is expected to give way 'by attenuation at few and distant places' [20]. While the latter case is extensively discussed in the literature [24,25], the former case is only discussed to my knowledge in Rayleigh's 1892 paper.
[28] The fastest-growing mode argument neatly side-steps the issue of whether the long-wavelength stability analysis misses a possible finite-wavelength instability, since the generic picture is expected to hold in both cases.
[29] An interesting corollary of this is that if *more* liquid is added to the final state, the amount contained in the groove should go *down*, since adding liquid increases the size of the large droplet and reduces its Laplace pressure (towards zero), thereby in parallel diminishing the filling depth of the liquid column contained in the channel.
[30] P. Concus and R. Finn, Proc. Natl. Acad. Sci. USA **63**, 292 (1969).
[31] K. Rejmer, S. Dietrich, and M. Napiórkowski, Phys. Rev. E **60**, 4027 (1999).
[32] A. O. Parry, C. Rascón, and A. J. Wood, Phys. Rev. Lett. **85**, 345 (2000).
[33] J. M. Romero-Enrique and A. O. Parry, New J. Phys. **9**, 167 (2007).

[34] A. Malijevský and A. O. Parry, Phys. Rev. Lett. **110**, 166101 (2013).
[35] B. J. Carroll, J. Colloid Interface Sci. **57**, 488 (1976).
[36] P. G. de Gennes, F. Brochard-Wyart, and D. Quéré, *Capillarity and Wetting Phenomena* (Springer, New York, 2004).
[37] K. A. Brakke, Exper. Math. **1**, 141 (1992); see http://facstaff.susqu.edu/brakke/evolver/evolver.html.
[38] P. B. Warren, Phys. Rev. Lett. **87**, 225702 (2001).
[39] D. Fan, S. P. Chen, L.-Q. Chen, and P. W. Voorhees, Acta Mater. **50**, 1895 (2002).
[40] K. Hejranfar and E. Ezzatneshan, Phys. Rev. E **92**, 053305 (2015).
[41] M. Brinkmann and R. Blossey, Eur. Phys. J. E **14**, 79 (2004).
[42] This is a corollary of Proposition 32 in Book III of Euclid's Elements.